A Morphology Model for the Cyber-physical Operation of a Remote Swabbing Robot

Li-Wei Yang, Ping-Lang Yen*

***Abstract*—Swabbing for the specimen is crucial in controlling the Covid-19 pandemic, but it occupies a lot of healthcare workers with dangerous (the risk of spit infection) and dull operations. Our lab developed a remote swabbing robot to complete the task safely and efficiently. Depth information is crucial for controlling the force in the swabbing process, ensuring patients' safety. Nevertheless, constrained by the oral cavity size, the sensors can only collect a part of the depth information. This research implements the Cyber-physical System concept on the robot to have comprehensive depth information. The system has an adaptable digital twin of the human oral cavity that can adapt according to the patient' s oral shape, achieving precise swabbing. The precise swabbing makes the swabbing process comfortable and effective. This elementary study creates a statistically averaged model based on eight samples and contains the morphing error under 4 mm. Further study will focus on expanding the samples to minimize the error.**

***Index Terms*—3D Slicer, Cyber-Physical System, Generalized Procrustes Analysis, Model Morphing, Principal Components Analysis**

I. Introduction

THE Covid-19 pandemic has caused millions of death and substantial economic losses around the globe. The pandemic control has become a desperate problem, in which early swabbing to contain the spread is crucial. Our lab proposes a remote oral/nasal swabbing robot: it reduces the risk of spit infection for healthcare workers and lessens the stress on the medical system.

The block diagram of the system is as Fig. 1. With the human-in-the-loop logic, the operators can utilize their knowledge in selecting the swabbing area and thus increase the success rate in swabbing. The streaming video and the virtual model would help operators aim for swabbing areas. The virtual model would also serve as the digital twin of the robot: it shows the robot' s position and orientation and serves as a training environment for operators.

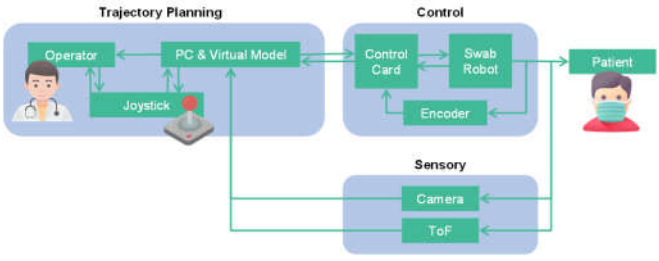

Fig. 1. System block diagram

The visual feedback of the current system is limited to A camera streaming, so it is hard for the operator to know the distance between the swab and the oral surface. Without the distance information, it is hard to control the swabbing force. We tried using an RGB-D camera to retrieve depth data, such as RealSense manufactured by Intel. Nevertheless, the operating hole is too narrow for RealSense to measure depth, as Fig 2. illustrates. We also considered tiny Time of Flight (ToF) sensors, but the distance information is too scarce to represent the swabbing area. As a result, we propose a method utilizing Computer Tomography (CT) images to gather most of the depth information preoperatively and use the information to build the statistically averaged human oral cavity model. In the swabbing process, we collect featured depth information using ToF, and utilize the information to morph the averaged model to fit the patient' s oral cavity. The morphed model would be shown to the operator, aiding the accuracy and the force control of the swabbing process.

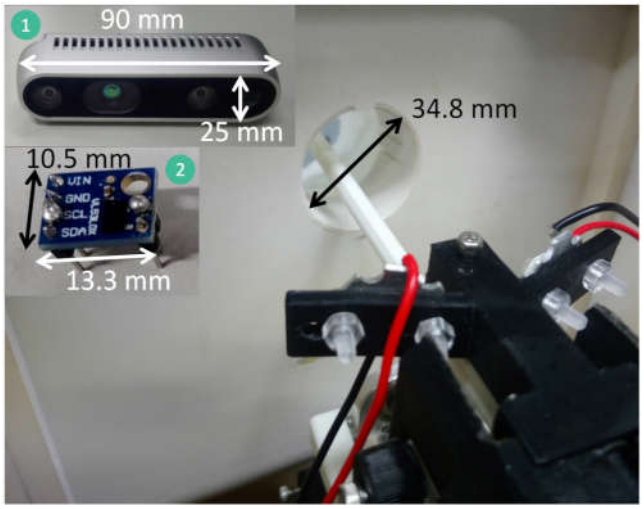

Fig. 2. Comparison of the size of two possible depth sensors and the operating hole. The operating hole on the shell is designed according to the comfortable size of human oral cavities. The hole is too narrow for RealSense (#1) to measure depth. On the other hand, if we adopt GY-530 ToF sensor (#2), it cannot provide holistic depth information around the swabbing area.

II. Related Work

Cyber-physical system (CPS) is an integrated system that combines software and hardware; it bridges the gap between the cyber (including communication, algorithm, and control) and the physical world (including mechanics, sensory, and actuation) [2]. The challenges of designing a CPS include: I. the hardware

This paper was submitted on October 10, 2022.
Part of this paper was orally presented at the 2022 International Conference on Advanced Robotics and Intelligent Systems (ARIS) [1]. This work was supported in part by Ministry of Science and Technology (MOST) in Taiwan under Grant 110-2813-C-002-379-E and 109-2622-E-002-021.

All authors are with Department of Biomechatronics Engineering at National Taiwan University, Taipei 106319, Taiwan (*Corresponding author: Ping-Lang Yen, e-mail: plyen@ntu.edu.tw).

part may change with time, making the model inaccurate, and II. the information is corrupted during transmission [3]. As a result, it is crucial to have a holistic view of system design to prevent grave errors. A Digital Twin would constantly extract information from the physical world to update itself and reach high fidelity even over a long period. The high fidelity enables the purpose of life prediction [4]. Reference [5] concludes the state-of-the-art development in Digital Twin: in addition to the above utility in Prognostic and Health Management, it can also solve problems like intelligent control, product optimization, and product flexibility.

Utilizing statistical methods to morph an average model to imitate a target is often used in computer-assisted orthopedic surgery. Reference [6] used this method for anterior cruciate ligament surgery. Its method can be divided into two stages: I. build the statistical model for the object, and II. fit the statistical model onto the target model using an optimization algorithm. In stage I. the authors used Octree Splines to register all the samples and subsequently used Principal Component Analysis (PCA) to record the statistical distribution of the samples. In stage II. the authors used the Nelder-Mead method along with the simulated annealing method to minimize the error. The initial solution of simulated annealing is generated using Iterative Closest Point (ICP) algorithm. The final Root Mean Square (RMS) error was around 0.4 mm. Reference [7] used the same staged structure on femoral heads, intending to provide a low-cost intra-operative model compared to CT or Magnetic Resonance Imaging (MRI). In stage I. the authors also used PCA to record the distribution. In stage II. the authors minimize an objective function by solving a linear system. The objective function incorporates Euclidean distance and Mahalanobis Shape Distance—a distance represents how far a sample is away from the mean. With leave-one-out experiments, the final error was around 1.5 mm.

The Genetic Algorithm (GA) is proposed by John Holland [8]. The method specializes in solving optimization problems. GA captured the concept of evolution to find the best solution—by introducing mechanisms like crossover, mutation, and fitness selection, the solution improves in each epoch [9]. In this research, we select GA as the optimization algorithm because it has multiple solution agents: it should be more efficient than the simulated annealing method with a single solution agent. The GA implemented in the research would generate multiple real numbers in one chromosome as the weights for the PCA morphing algorithm.

3D Slicer [10] is a data visualization software specializing in medical images. In this research, we modified the SlicerMorph [11] extension of 3D Slicer to meet our need for statistical morphing. 3D Slicer has multiple types of Fiducial Marker to mark crucial positions in the image. One of the Fiducial Markers is called Fiducial Markups; in later sections, we called it Markups. A Markups is a set of multiple Control Points; a Control Point can provide 3-dimensional coordinates data of a particular anatomical position. The Generalized Procrustes Analysis (GPA) submodule in SlicerMorph uses GPA to align Markups and get the average Control Points distribution, then uses PCA to extract the principal components of the distribution. We could morph the Control Points along the corresponding eigenvectors with the principal components. In this research, we adjust the weights of the cumulative top 90% importance of the principal components. The values of these weights are obtained from GA, and they minimize the Euclidean distance between the target and the morphed Markups.

III. METHODS

In the following section, GPA and PCA Morphing (parts C and D) belong to SlicerMorph [11] extension. Before entering these two parts, we preprocess our data (parts A and B) to produce better input for later parts. We incorporate GA (part E) in PCA Morphing to optimize the morphing parameters, and lastly, we put the final result in CPS simulation (part F).

A. Data Preprocessing

After obtaining the CT data from the dentistry, we use the Volume Rendering module to render the CT image to ensure the Region of Interest (ROI) is captured; we then use the Volume module to center the volume onto the origin of the space. At this point, the volume' s orientation and position still

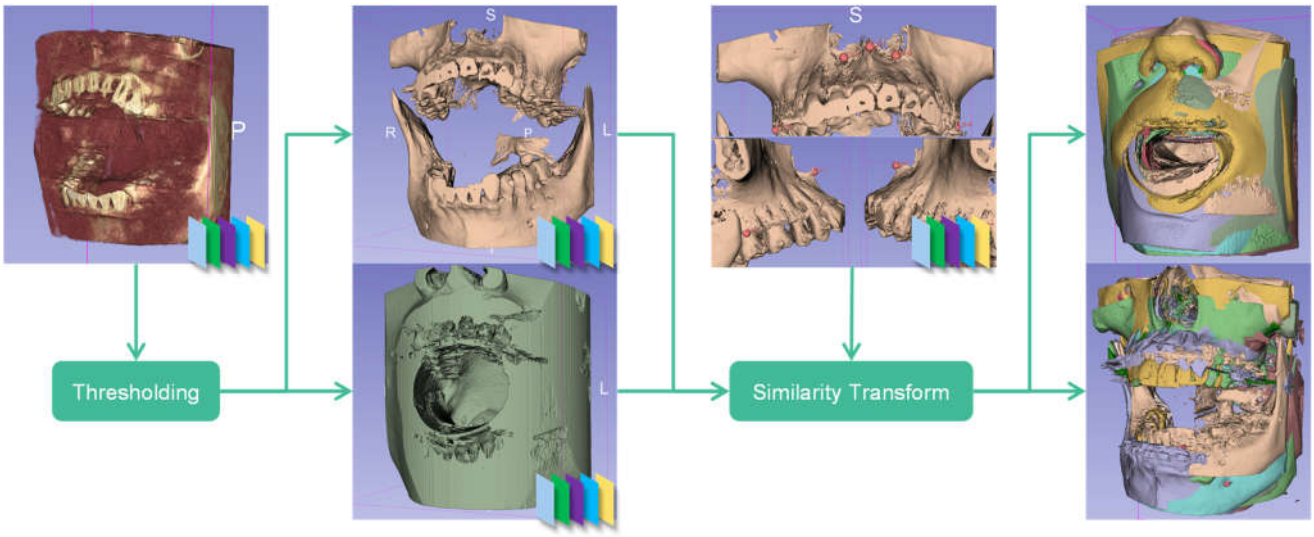

Fig. 3. Data Preprocessing flow chart. Once the hard tissue is segmented, we place Markups on it to generate Similarity Transform to register the hard tissue and soft tissue. The graphs with little icons mean batch operation (the operation is done for every sample).

require further alignment using Markups. Therefore, we first need to segment the CT to have a model that has a concrete surface to place Markups. We use Segmentation Editor to threshold the image. The whole process is shown in Fig. 3. Because soft tissue is unstable, the Markups placed upon the soft tissue are not stable enough to register these samples. As a result, we use different threshold settings to segment the hard tissue from the soft tissue and place Markups upon the hard tissue to register these samples. The registration transformation used is Similarity Transform: through rotation, scaling, and affine to register samples. Here we choose sample 7 as the registration target because the image quality of sample 7 is the best.

Table I shows the RMS error of the transform. Afterward, we apply these transforms onto the soft tissue to complete the registration process. The soft tissue threshold selection here is based on Global Otsu [12]; as for hard tissue, the threshold selection is arbitrary: as long as it separates the hard tissue from the soft tissue. The soft tissue model may contain artifacts, so we use different tools to clean the soft tissue data, as shown in Fig 4.

TABLE I
RMS ERROR IN SIMILARITY TRANSFORM OF MARKUPS

Item No.	RMS Error (mm) [a]
1	2.43
2	1.50
3	0.94
4	2.25
5	1.79
6	2.09
7	0.00
8	1.99

[a] Round up to the hundredth digit

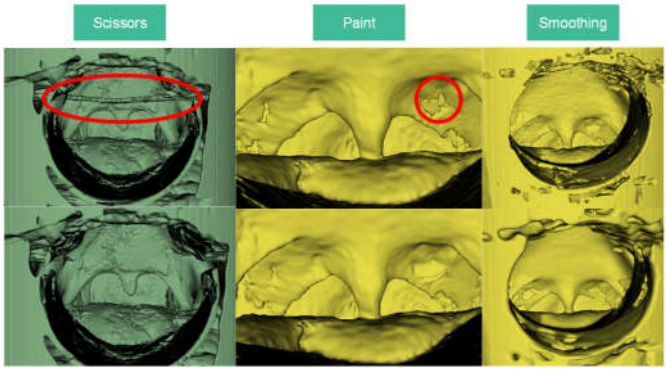

Fig. 4. Soft tissue data cleaning tools. For noise, we use Scissors to cut off; for holes, we use Paint to fill them up. We also smooth the model for later Markups placement, using a median filter with a 2 mm^3 kernel size.

B. Placement of Markups

In this research, we place two sets of Markups for each sample: one is placed upon hard tissue to generate similarity transform for registration, and the other is placed upon soft tissue to capture the depth information around the swabbing area. The first set has five Control Points: the first three are placed around Anterior Nasal Spine, and the rest are placed upon the Buccal Cervical Root of the Left and Right Maxillary Second Molar. The second set also has five Control Points: they are placed upon the Uvular and the Palatoglossal Arch—the swabbing areas selected by doctors and in [13] indicates. By combining these two sets, we can get the Markups used in the algorithm later. Fig 5. shows the position of the Control Points. Because we want to match the scarce depth data obtained by the ToF sensor, we place relatively sparse Control Points; on the other hand, it is to prevent irrelevant data from tampering with the model' s accuracy.

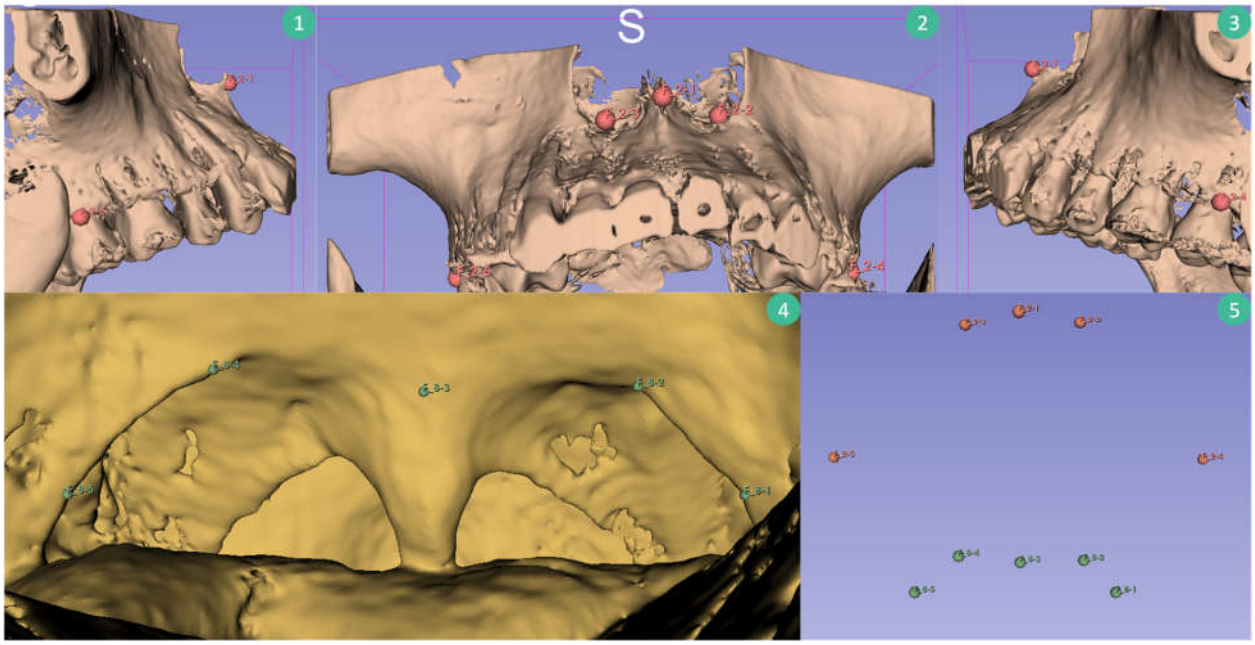

Fig. 5. No. 1, 2, and 3 are the views from the front, right, and left of the Control Points for the hard tissue. No. 4 is the front view of Control Points for the soft tissue. No. 5 is the front view of combined Markups for the later morphing algorithm.

C. Generate Average Markups

With the combined Markups, we first conduct GPA to construct the average Markups. Let us have N Markups, and each Markups has K Control Points. GPA first subtracts the mean from each Control Point' s coordinates to have initial alignment.

$$\boldsymbol{A} = \{A_n \in \boldsymbol{A} | 1 \le n \le N\} \quad (1)$$

$$A_n = \{{}^nP_1, \cdots, {}^nP_K\} \quad (2)$$

$${}^nP_k = ({}^nx_k, {}^ny_k, {}^nz_k) \quad (3)$$

Where **A** is the set of all Markups, A_n is one of the Markups, ${}^nP_k$ is a point in A_n , $({}^nx_k, {}^ny_k, {}^nz_k)$ is the corresponding coordinates.

The initial alignment would turn A_n to A_n':

$$A_n \to A_n' = \{{}^nP_1', \cdots, {}^nP_K'\} \quad (3)$$

$${}^nP_k' = {}^nP_k - (\bar{x}_k, \bar{y}_k, \bar{z}_k) \quad (4)$$

$$\bar{x}_k = \frac{\sum_{n=1}^{N} {}^nx_k}{N}, \bar{y}_k = \frac{\sum_{n=1}^{N} {}^ny_k}{N}, \bar{z}_k = \frac{\sum_{n=1}^{N} {}^nz_k}{N} \quad (5)$$

The first sample' s Markups would then be considered the initial average Markups. We multiply the transpose of the first Markups and the rest Markups, and we take Singular Value Decomposition on the result to get two unitary matrices, U and V^*. We take the transpose of the two and multiply them together to get the rotational matrix that can align this sample with the first sample and times the Markups with the rotational matrix to align them even further. Let the second Markups be A_2', the whole process is as follows:

$$A_1'^T A_2' = U\Sigma V^*, R = V^{*T}U^T, A_2'' = A_2'R \quad (6)$$

Where A_2'' is the Markups that are aligned with A_1'.

When the process was over, we averaged the coordinates again along with the first dimension to get the initial average Markups, M, as below:

$$M = \{\tilde{P}_1, \cdots, \tilde{P}_K\} \quad (7)$$

$$P_k = (\tilde{x}_k, \tilde{y}_k, \tilde{z}_k) \quad (8)$$

Where P_k is a point in M,$(\tilde{x}_k, \tilde{y}_k, \tilde{z}_k)$ is the corresponding initial mean coordinates.

With the method mentioned above, we align all the samples with this initial average Markups again. The process would go iterative until a particular round when the Frobenius norm of the difference between averaged Markups this round and the previous one is less than 0.0001. Then we get the final averaged Markups, M'. This Markups would later be used in the PCA morphing algorithm. The whole process is illustrated in Fig. 6.

After GPA, we could also know each sample' s Procrustes distance, representing the sample' s distance always from the mean. As Table II shows, sample 7 is the closest sample to the mean; it would be the morphing template in later PCA morphing.

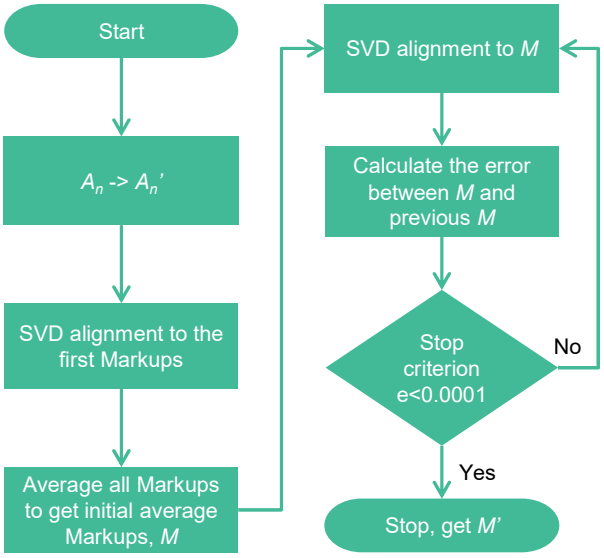

Fig. 6. GPA flow chart.

TABLE II
PROCRUSTES DISTANCE OF SAMPLES

Item No.	Procrustes Distance (mm) [a]
7	6.72
4	7.66
8	8.29
2	9.60
6	11.81
1	12.34
3	14.82
5	18.39

[a] Round up to the hundredth digit

D. PCA Morphing Algorithm

We take the aligned samples running the PCA. We can get eigenvectors. By changing the weights of these eigenvectors, we could morph the average Markups, M', as below equation:

$$m = M' + \sum_{i=1}^{t} w_i e_i \quad (9)$$

Where e_i is eigenvector, w_i is the corresponding weight, m is the morphed Markups, t is the number of eigenvectors in use.

In the research, we select the cumulative top 90% importance of the eigenvector as the morphing direction, as Table III shows. (to PC3, so t is 3)

TABLE III
CUMULATIVE SIGNIFICANCE OF EIGENVECTORS

No.	Eigenvalue [a]	Percentage (%)[a]	Cumulative Percentage (%)[a]
PC1	71.43	51.30	51.30
PC2	33.15	23.80	75.10
PC3	14.46	10.40	85.50
PC4	12.59	9.00	94.50
PC5	5.14	3.70	98.20
PC6	1.61	1.20	99.40
PC7	0.96	0.70	100
PC8	0.00	0.00	100

[a] Round up to the hundredth digit

We select Markups No. 7 as the morphing template since it is the closest sample to the mean. No. 7 would first calculate the Bookstein Thin-plate Spline transform [14] with the averaged Markups, M'. The transformation can fit the template Markups onto the averaged Markups; the objective function is as below:

$$E_{tps,smooth}(f) = \sum_{i=1}^{k} \| t_i - f(x_i) \|^2 + \lambda J_o^d(f) \quad (10)$$

Where $E_{\text{tps,smooth}}(f)$ is the value we seek to minimize, f is the target function, x_i is the control point of the morphed Markups, t_i is the control point of the target Markups, λ is a rigidity controlling factor, $J_o^d(f)$ is the gradient of f on each dimension.

If we apply the transformation to the model of the template, then we get our initial template model. When the template Markups are morphed by the PCA algorithm mentioned earlier, the model would also be warped by the Markups, thus morphing the model.

E. Genetic Algorithm

The genetic algorithm finds the correct weights of principal components to morph the Markups closest to the target Markups. The selection method is deterministic: we select the top N of the population pool to get into the next epoch. This selection method is more efficient than Probability Proportional Stochastic Selection. The hyperparameters are set according to Table IV.

TABLE IV
GENETIC ALGORITHM HYPERPARAMETER SETTINGS

Item	Symbol	Settings
Population Size	N	100
Crossover Rate	Cr	0.8
Mutation Rate	Mr	0.2
Dimension	D	3
Upper/Lower Bound	B	6
Max Epoch	Me	500

We select the principal components that sum up to 90% (PC1~PC3). Initialize the pool with N chromosome—every chromosome contains D real numbers (here, D = 3 because we select three principal components) as the weights of the PCA morphing algorithm. The range of generated real numbers is between -32 to +31, which is constrained by B ($-2^{B-1} \sim 2^{B-1}-1$). The number of iterative epochs is set at 500 epochs. The objective function is the RMS error between the target Control Points and the morphed Control Points. The GA would evolve to minimize the objective function value O.

F. CPS Simulation

In this research, we adopt the method in [15]; after generating an assembly in SOLIDWORKS, we use sw2urdf extension to turn the assembly into URDF (Unified Robot Description Format). URDF cannot simulate closed kinematic chains, so we open the URDF using Gazebo, add joints in the model editor to fulfill the closed kinematic chains, and save the file as SDF (Simulation Description Format). Fig. 7 shows the result. Aside from the robot, we use the same method to generate the morphed oral model. However, the oral model has too many triangulated surfaces for Gazebo to handle, and thus we only crop out the necessary region and show it in the simulation.

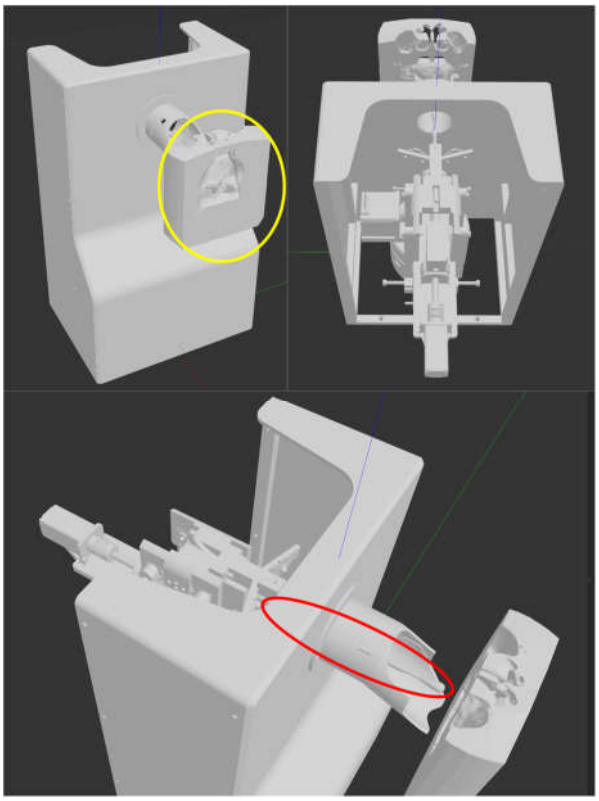

Fig. 7. Gazebo simulation. The yellow circle indicates the position of the oral model, whereas the red circle points out the swab rod mounted on the robot.

IV. RESULT

We use the input Markups as the morphing target because the data transfer between the ToF sensor and the algorithm module has not been set. Table V lists the RMS error in the Euclidean distance of morphing the average Markups to the target Markups; the table shows that we contained the RMS error below 4 mm, not a satisfying result compared to the 0.4 mm error achieved in [6]. However, [6] conducts this morphing structure on rather stable hard tissue, whereas we are the first to adopt this method on unstable soft tissue. Fig. 8 shows the morphed results of Markups, while Fig. 9 shows the morphed result of the model. The two figures mentioned above show that the swabbing region: the Uvular and the Palatoglossal Arch, are aligned at the same depth.

TABLE V
RMS ERROR OF MORPHING MARKUPS

Item No.	RMS Error (mm)[a]
1	0.92
2	3.80
3	1.23
4	4.04
5	1.06
6	2.44
7	1.79
8	1.44

[a] Round up to the hundredth digit

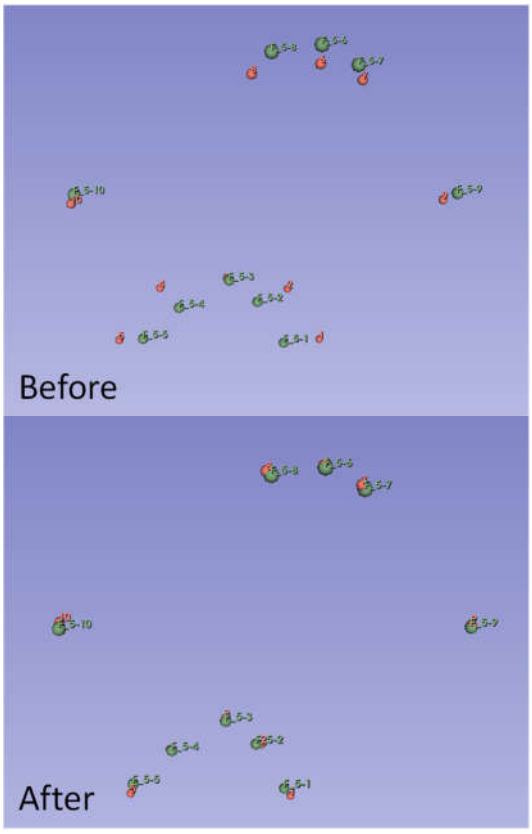

Fig. 8. The morphing result of Markups of sample 5. The red Markups are the morphed Markups, whereas the green Markups are the target.

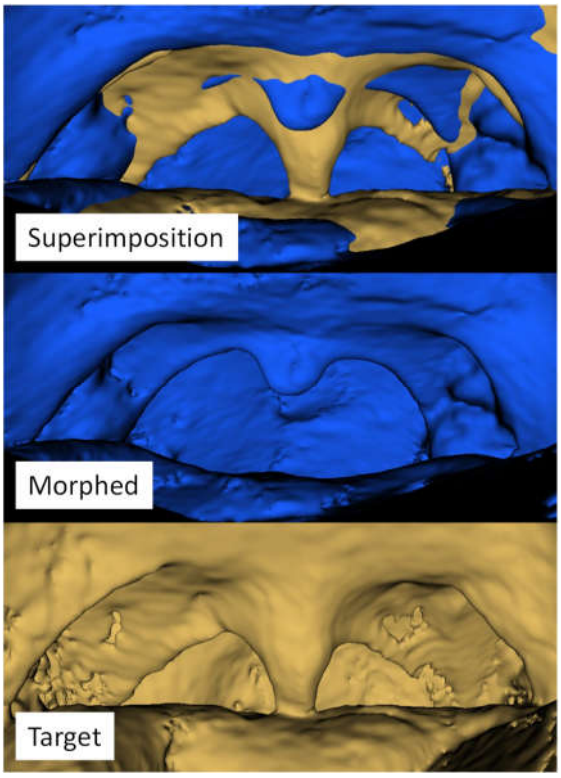

Fig. 9. The morphing result of model of sample 8. The upmost graph shows the superimposition of the morphed model (in blue) and the target model (in yellow). The two lower graphs show the models respectively.

V. Conclusions

This research proposes a CPS incorporating the statistically averaged human oral cavity and containing the final error below 4 mm. We got only ten CT data, of which two are of terrible quality, so they were not used in the research. The size of the dataset is too small to put the method into practice. In a further study, we will expand our dataset and focus on changing the number and position of the Markups to see if we can improve the result.

Acknowledgment

The CT data in this work were captured by Compson Dental Clinic, New Taipei City, Taiwan; with samples from members of Robots and Medical Mechatronics Lab (RMML). The Genetic Algorithm in this work was completed with the assistance of professor Feng-Cheng Yang, Institute of Industrial Engineering, National Taiwan University.

References

[1] Li-Wei Yang, Ping-Lang Yen, "Smart Cyber-physical System of a Remote Swabbing Robot," International conference on Advanced Robotics and Intelligent Systems, 2022

[2] M. N. Sadiku, Y. Wang, S. Cui, and S. M. Musa, "Cyber-physical systems: a literature review," European Scientific Journal, vol. 13, no. 36, pp. 52-58, 2017.

[3] P. Derler, E. A. Lee, and A. S. Vincentelli, "Modeling Cyber–Physical Systems," Proceedings of the IEEE, vol. 100, no. 1, pp. 13-28, 2012, doi: 10.1109/jproc.2011.2160929.

[4] S. Boschert and R. Rosen, "Digital Twin—The Simulation Aspect," Springer International Publishing, 2016, pp. 59-74.

[5] F. Tao, H. Zhang, A. Liu, and A. Y. C. Nee, "Digital Twin in Industry: State-of-the-Art," IEEE Transactions on Industrial Informatics, vol. 15, no. 4, pp. 2405-2415, 2019, doi: 10.1109/tii.2018.2873186.

[6] M. Fleute, S. Lavallée, and R. Julliard, "Incorporating a statistically based shape model into a system for computer-assisted anterior cruciate ligament surgery," Medical Image Analysis, vol. 3, no. 3, pp. 209-222, 1999/09/01/ 1999, doi: https://doi.org/10.1016/S1361-8415(99)80020-6.

[7] K. T. Rajamani, S. C. Joshi, and M. A. Styner, "Bone model morphing for enhanced surgical visualization," IEEE, doi: 10.1109/isbi.2004.1398773.

[8] J. H. Holland, "Genetic Algorithms," Scientific American, vol. 267, no. 1, pp. 66-73, 1992

[9] S. Mirjalili, "Genetic Algorithm," Springer International Publishing, 2019, pp. 43-55.

[10] S. Pieper, M. Halle, and R. Kikinis, "3D Slicer," IEEE, doi: 10.1109/isbi.2004.1398617.

[11] S. Rolfe et al., "SlicerMorph: An open and extensible platform to retrieve, visualize and analyze 3D morphology," Cold Spring Harbor Laboratory, 2020.

[12] N. Otsu, "A Threshold Selection Method from Gray-Level Histograms," IEEE Transactions on Systems, Man, and Cybernetics, vol. 9, no. 1, pp. 62-66, 1979, doi: 10.1109/tsmc.1979.4310076.

[13] P. Di Maio, O. Iocca, A. Cavallero, and M. Giudice, "Performing the nasopharyngeal and oropharyngeal swab for 2019-novel coronavirus (SARS-CoV -2) safely: How to dress, undress, and technical notes," Head & Neck, vol. 42, no. 7, pp. 1548-1551, 2020, doi: 10.1002/hed.26230.

[14] F. L. Bookstein, "Principal warps: thin-plate splines and the decomposition of deformations," IEEE Transactions on Pattern Analysis and Machine Intelligence, vol. 11, no. 6, pp. 567-585, 1989, doi: 10.1109/34.24792.

[15] M. Bailey, K. Gebis, and M. Žefran, "Simulation of Closed Kinematic Chains in Realistic Environments Using Gazebo," Springer International Publishing, 2016, pp. 567-593.